

pubs.acs.org/acscatalysis Research Article

# Accelerated Cu<sub>2</sub>O Reduction by Single Pt Atoms at the Metal-Oxide Interface

Alex C. Schilling, Kyle Groden, Juan Pablo Simonovis, Adrian Hunt, Ryan T. Hannagan, Volkan Çınar, Jean-Sabin McEwen, E. Charles H. Sykes, and Iradwikanari Waluyo\*



Cite This: ACS Catal. 2020, 10, 4215-4226



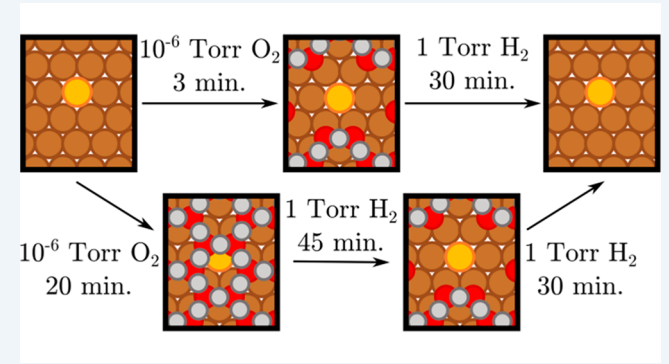
**ACCESS** 

III Metrics & More

Article Recommendations

s Supporting Information

ABSTRACT: The reducibility of metal oxides, when they serve as the catalyst support or are the active sites themselves, plays an important role in heterogeneous catalytic reactions. Here we present an integrated experimental and theoretical study that reveals how the addition of small amounts of atomically dispersed Pt at the metal/oxide interface dramatically enhances the reducibility of a Cu<sub>2</sub>O thin film by H<sub>2</sub>. X-ray photoelectron spectroscopy (XPS) and temperature-programmed desorption (TPD) results reveal that, upon oxidation, a PtCu single-atom alloy (SAA) surface is covered by a thin Cu<sub>2</sub>O film and is, therefore, unable to dissociate H<sub>2</sub>. Despite this, *in situ* studies using ambient-pressure (AP) XPS reveal that the presence of a small amount of Pt under the oxide layer can, at the single-atom limit,



promote the reduction of  $Cu_2O$  by  $H_2$  at room temperature. We built two density functional theory based surface models to better understand these experimental findings: a  $Cu_2O/Cu(111)$ -like surface oxide layer, known as the "29" oxide, in which Pt is alloyed into the Cu(111) surface, as well as a PtCu SAA. Our calculations suggest that the increased activity is due to the presence of atomically dispersed Pt under the surface oxide layer, which weakens the Cu-O bonds in its immediate vicinity, thus making the interface between subsurface Pt and the surface oxide a nucleation site for the formation of metallic Cu. This initial step in the reduction process results in the presence of surface Pt atoms surrounded by metallic Cu patches, and the Pt atoms become active in  $H_2$  dissociation, which consequently accelerates the reduction of the oxide layer. This work demonstrates how isolated Pt atoms at the metal/oxide interface of a Cu-based catalyst accelerate the reduction of the oxide and, therefore, help maintain the active, reduced state of the catalyst under the reaction conditions.

**KEYWORDS:** single-atom alloy, copper oxide reduction, hydrogen activation, metal/oxide interfaces, ambient-pressure X-ray photoelectron spectroscopy, density functional theory

## ■ INTRODUCTION

The production of methanol in the United States has increased by 45% in the last half decade, with each methanol plant in the US producing up to 1.5 million tons of methanol per year from CO<sub>2</sub>. 1-3 Methanol production requires the dissociation of H<sub>2</sub> in order to provide accessible surface hydrogen for the reduction of adsorbed CO<sub>2</sub>. Typically, supported Cu catalysts are used for this reaction. While various supports play a crucial role in the ultimate formation of methanol, their exact role in the overall synthesis mechanism has been widely debated. In the past, these supports have been shown to keep Cu dispersed, provide charge transfer to Cu sites, and aid in hydrogen spillover and storage during methanol synthesis. 13,14 A number of studies have also cited strain between the Cu and support caused by a lattice mismatch as the reason for the increased catalytic performance. 11,15,16 This latter point is further supported through a 2007 study by Kasatkin et al. that reported an increase in nonequilibrium Cu structures (likely with a high degree of lattice mismatch) led to increased catalytic activity.  $^{17}$ 

Most recently, studies have theorized that interface sites between the Cu and the support are the active sites for methanol synthesis.  $^{9,17-21}$  In 2014, Bonura et al. demonstrated this finding by preparing three different catalysts with varying Cu loadings and oxide coverages. The results indicated that the catalytic activity scales with the number of interfacial sites that allows for both  ${\rm CO}_2$  activation and  ${\rm H}_2$  dissociation. These interfacial sites are crucial to the ability of the catalyst to function, but there is a possibility of these sites being covered

Received: December 5, 2019 Revised: March 3, 2020 Published: March 9, 2020



due to oxide growth on the metallic copper, a process which by itself has been studied by a number of groups extensively.  $^{22-24}$  Integration of precious-metal dopants into these interface regions could facilitate  $H_2$  dissociation and hence maintain the reduced state necessary for catalytic functionality,  $^{25-28}$  thereby significantly improving the cyclability of these catalysts. The reduction kinetics and  $H_2$  dissociation at these doped interface regions have yet to be studied at a level of detail necessary to direct the rational design of more efficient methanol synthesis catalysts using this methodology.

Specific to this work, the reduction of Cu<sub>2</sub>O by various gases has been extensively studied using in situ methods.<sup>29,30</sup> CO is known to be able to easily reduce a Cu2O thin film under relatively mild conditions (10 mTorr at room temperature) via the Mars-van Krevelen mechanism, 31,32 and the addition of potassium dopants on the surface has been found to accelerate the reaction. 30,33 In these cases, the reduction was found to start on defect sites, both on step edges and on terraces. The reduction of Cu<sub>2</sub>O by H<sub>2</sub>, on the other hand, is less facile due to the requirement for H2 dissociation, which has a high activation energy on the pristine Cu<sub>2</sub>O surface. <sup>29,34</sup> The presence of defects and O vacancies on the Cu2O surface can decrease the activation energy for H2 dissociation, but the presence of platinum-group metals, with their low dissociation barriers, could yield a more significant effect.<sup>35</sup> For example, the addition of a small amount of Pt to a Cu(111) surface forms a single-atom alloy (SAA) in which platinum is atomically dispersed in the first layer of Cu. These isolated Pt atoms have been shown to be highly active in H<sub>2</sub> dissociation, with the added benefit that they are more resistant to CO poisoning in comparison to Pt nano-particles. 26,28,36

In this study, we use the SAA approach to dope the interface of a Cu metal/Cu<sub>2</sub>O model system and examine H<sub>2</sub> dissociation and subsequent oxide reduction at these metal sites through a combination of in situ ambient-pressure experiments, ultrahigh-vacuum (UHV) studies, and density functional theory (DFT) based calculations. Our model catalyst is inspired by, and made similarly to, the previously studied "29" oxide, which has been characterized by Therrien and co-workers.<sup>37</sup> The structure contains six hexagonal oxide rings that are slightly distorted, five of which have an oxygen adatom in the center. The unit cell is 29 times larger than a Cu(111) unit cell and is typically prepared by oxidizing a Cu surface at 650 K. In this work, Pt dopants are introduced prior to oxidation by depositing Pt on the bare Cu substrate at 380 K to first form the well-known PtCu(111) SAA. 26,28 After oxidation at 400 K, the resulting oxide layer likely resembles the "29" oxide due to similarities in preparation methods as well as experimental evidence from X-ray photoelectron spectroscopy (XPS) and CO desorption data. To leverage the strength of each technique, we employed in situ ambientpressure (AP) XPS to study the reducibility of the Pt-doped Cu<sub>2</sub>O surface in near-ambient pressures of H<sub>2</sub> in comparison to that of the bare surface, and to understand the role of Pt, we examined the reactivity of the surface toward H2 dissociation using UHV experiments with temperature-programmed desorption (TPD). Low-energy electron diffraction (LEED) was used to assess the order of the oxide after different UHV treatments. Finally, we used DFT-based calculations to provide atomistic insight into the experimentally observed dissociation and reduction processes.

#### METHODS

Ambient-Pressure X-ray Photoelectron Spectroscopy (AP-XPS). AP-XPS experiments were performed at the 23-ID-2 (IOS) beamline at the National Synchrotron Light Source II (NSLS-II) at Brookhaven National Laboratory (BNL). Details about the endstation and experimental setup have been described elsewhere.<sup>38</sup> Cu(111) was cleaned using repeated cycles of Ar<sup>+</sup> sputtering (1 kV in  $5 \times 10^{-5}$  Torr of Ar for 20 min) and annealing to 850 K for 15 min. Pt was deposited using a SPECS EBE-4 e-beam evaporator at a deposition rate of a 0.025 (2.5%) monolayer equivalent (MLE)/min at a sample temperature of 370-380 K. The evaporator was first calibrated with a quartz crystal microbalance, and the absolute coverage of Pt was determined by monitoring the attenuation of the Cu 2p peak. O<sub>2</sub> (Matheson, ultrahigh purity, 99.98%), CO (Matheson, research purity, 99.999%), and H<sub>2</sub> (Matheson, ultrahigh purity, 99.999%) were introduced into the chamber during experiments using separate variable leak valves, and the pressure was monitored by a hot cathode ion gauge/Pirani gauge combination at low pressures (below 1 mTorr) and a capacitance manometer above 1 mTorr.

Pt 4f and O 1s spectra were obtained at 250 and 710 eV photon energies, respectively. Cu 3p was used for energy calibration at each photon energy. During experiments at an ambient pressure of H<sub>2</sub>, the photon flux was reduced by detuning the undulator to eliminate any possible beaminduced reaction. The absence of beam-induced effects was confirmed by checking different spots on the sample as well as by performing a "dark" experiment: i.e., without exposure to X-ray photons.

Temperature-Programmed Desorption (TPD). The UHV TPD experiments presented in this work was performed on a Cu(239 241 246) single crystal with (111) terraces of ~17 nm width and R kinked step edges,<sup>39</sup> which closely resembles a Cu(111) crystal. The TPD chamber has a base pressure of  $<1 \times 10^{-10}$  Torr. The chamber utilizes a Hiden quadrupole mass spectrometer (Hal RC 201) and a manipulator equipped with a liquid nitrogen cryostat capable of cooling the crystal to 85 K and resistive heating able to heat the crystal to 750 K. The crystal was cleaned via Ar<sup>+</sup> sputtering followed by a 750 K anneal. The Pt/Cu<sub>2</sub>O surface was prepared by depositing Pt using a Focus GmbH EFM3 electron beam evaporator on the clean Cu crystal held at 380 K. This PtCu alloy was heated to 400 K and exposed to O<sub>2</sub> gas (USP grade; Airgas) at 5  $\times$   $10^{-6}$  Torr for 3 and 20 min. For the sputtered surface, an RBD sputter gun with a filament current of 4 A, a focus of 0, and a beam energy of 500 V was used for 1 min with a drain current of 0.7  $\mu$ A. Low-energy electron diffraction (LEED) patterns (OCI Vacuum Microengineering) were used to confirm the surface structure of each sample. The samples were exposed to CO (99.99%; Airgas) and H<sub>2</sub> (99.9%; Airgas) through high-precision leak valves. All TPD experiments were performed with a 1 K/s linear heating rate. An analysis of the TPD peaks accounts for the ionization cross section, quadrupole mass spectrometer sensitivity, and fragmentation pattern of desorbing species.

Density Functional Theory Calculations. All quantum-mechanical calculations were performed using the Vienna ab initio simulation package (VASP).<sup>40,41</sup> Interactions between core and valence electrons were treated with the projector-augmented wave (PAW) method<sup>42</sup> using data sets released by VASP in 2012. Electronic exchange and correlation energies

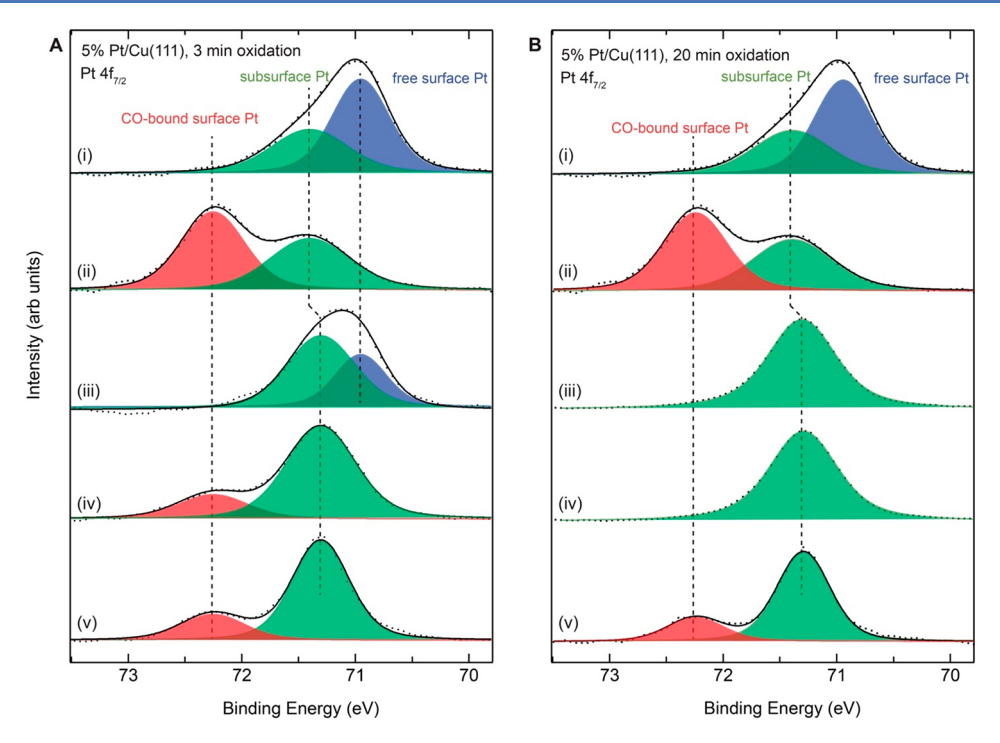


Figure 1. Pt  $4f_{7/2}$  XPS spectra of 5% PtCu(111) before and after oxidation for (A) 3 min, and (B) 20 min: (i) as-deposited surface, measured under UHV at 300 K; (ii) as-deposited surface, under  $1 \times 10^{-4}$  Torr of CO at 300 K; (iii) after oxidation under  $5 \times 10^{-6}$  Torr of  $O_2$  at 400 K, measured under UHV; (iv) oxidized sample, under  $1 \times 10^{-4}$  Torr of CO at 300 K; (v) after reduction of the oxide by  $H_2$ , measured under  $1 \times 10^{-4}$  Torr of CO at 300 K.

were computed using the Perdew–Burke–Ernzerhof functional. A cutoff energy of 500 eV was used to determine the size of the plane-wave basis set used at each sampled k point. Unless otherwise specified, Gaussian smearing was used in all calculations using a smearing width of 0.2 eV. In all calculations, self-consistent field cycles were considered complete once the total electronic energy changed by less than  $10^{-6}$  eV between subsequent iterations. Further, geometries were considered optimized once Cartesian forces were less than 0.02 eV/Å for all relaxed Cartesian coordinates.

Minimum energy pathway calculations were performed using the climbing-image nudged elastic band (CINEB) method, 44,45 using anywhere between three and five images for an elementary step. These calculations were considered converged once the relevant projected forces on all relaxed Cartesian coordinates in each image were below 0.02 eV/Å. For each elementary step, the vibrational modes of the saddlepoint structure were computed, using in-house software wrapped around VASP, to confirm the presence of a single imaginary mode to satisfy the strict definition of a transition state.

A variety of surfaces were used for the calculations presented in this work. Adsorption calculations of oxygen and hydrogen were carried out on  $p(4\times4)$  supercells of Pt(111) and Cu(111) that were four atomic layers thick. The bulk lattice constants were determined to be 3.968 and 3.635 Å for Pt and Cu, respectively, where  $20\times20\times20$  and  $12\times12\times12$  Monkhorst–Pack grids were used, respectively. Additionally, oxygen adsorption calculations were carried out on a PtCu(111) SAA. This surface was constructed by substituting one of the Cu atoms in the top layer of a four-layer-thick  $p(4\times4)$  Cu(111) supercell (with a lattice constant of 3.635 Å) with a Pt atom. A  $3\times3\times1$  Monkhorst–Pack grid was used to sample the first Brillouin zone for all of these surfaces, and the

bottom two layers were held fixed in their bulk positions. Note that the calculations involving oxygen adsorption were spin-polarized. To generate densities of states, a single-point calculation was performed using a  $11 \times 11 \times 1$  Monkhorst—Pack grid and tetrahedron smearing using the geometries optimized via the previously mentioned protocol. The band centers in these plots were computed through integration over only occupied electronic states using the following formula, where E is the electronic energy,  $\varepsilon_{\rm center}$  is the band center,  $\rho(E)$  is the electronic density of states, and  $E_{\rm Fermi}$  is the Fermi energy:

$$\varepsilon_{\text{center}} = \frac{\int_{-\infty}^{E_{\text{Fermi}}} E\rho(E) \, dE}{\int_{-\infty}^{E_{\text{Fermi}}} \rho(E) \, dE}$$
(1)

As a theoretical model for oxidized PtCu(111), a slightly modified "29" Cu<sub>x</sub>O/Cu(111) surface was used. The unmodified "29" Cu<sub>x</sub>O/Cu(111) surface, less formally known as the "29" oxide, is experimentally formed by oxidizing Cu(111) at 650 K and has been observed by multiple groups. The theoretical unit cell used to model this surface consists of a Cu(111) surface supercell, consisting of 4 atomic layers with 29 Cu atoms each, topped with 6 hexagonal, Cu<sub>2</sub>O-like rings and 5 additional oxygen adatoms. This cell's construction is detailed elsewhere, where it is vetted thoroughly against experimental images.<sup>37</sup> This base surface was modified for this study by swapping one of the Cu atoms in the top Cu(111) layer with a Pt atom to reflect the oxidation of a PtCu(111) surface instead of just a Cu(111) surface. Due to this cell's large size (approximately an 18 Å  $\times$  9 Å rectangle), a 1 × 2 × 1 Monkhorst-Pack grid was sufficient for the first Brillouin zone sampling during geometry optimizations. However, to generate densities of states, single-point

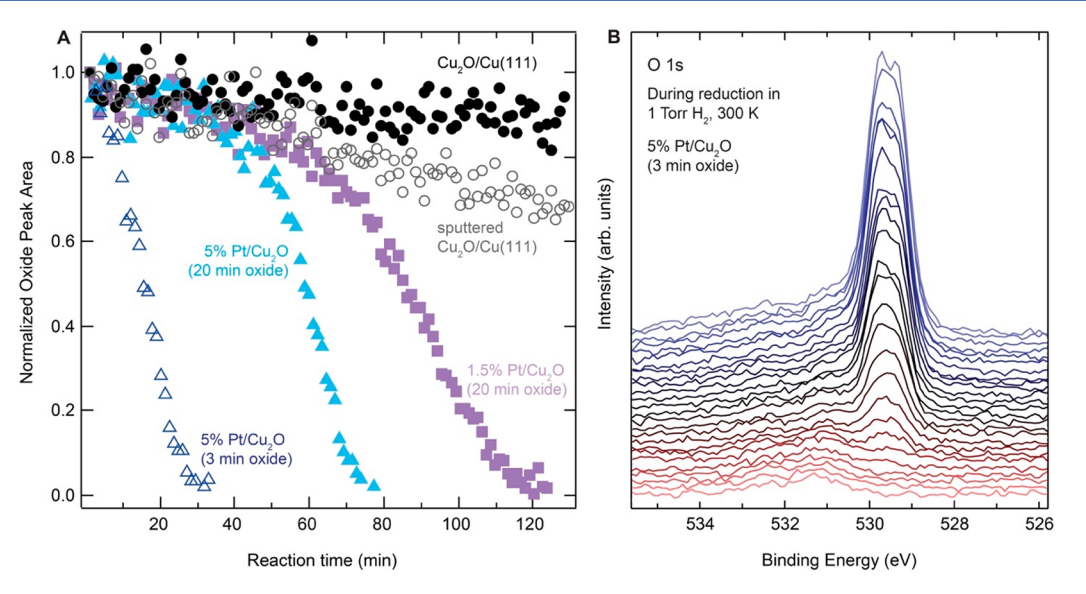


Figure 2. (A) Plot of normalized oxide peak area as a function of reaction time in 1 Torr of  $H_2$  at 300 K for bare  $Cu_2O/Cu(111)$  (closed circles), lightly sputtered  $Cu_2O/Cu(111)$  (open circles), 1.5%  $Pt/Cu_2O(20 \text{ min})$  (squares), 5%  $Pt/Cu_2O(20 \text{ min})$  (closed triangles), and 5%  $Pt/Cu_2O(3 \text{ min})$  (open triangles). (B) O 1s AP-XPS spectra during the reduction of 5%  $Pt/Cu_2O(3 \text{ min})$  under 1 Torr of  $H_2$  at 300 K. Spectra were acquired every 70 s.

calculations using a  $3 \times 6 \times 1$  Monkhorst–Pack grid and tetrahedron smearing were performed.

## RESULTS

In Situ Surface Characterization and Reactivity Studies with AP-XPS. Figure 1 shows the Pt  $4f_{7/2}$  XPS spectra of 5% Pt deposited on the Cu(111) surface under UHV and exposed to a variety of conditions. The as-deposited surface measured under UHV, shown in spectra i in Figure 1A,B, can be fitted with two components: namely, the free (i.e., unbound to any adsorbates) surface Pt atoms embedded in the first layer of Cu(111) at 70.95 eV and subsurface Pt atoms at 71.4 eV. $^{38,48}$  The former component is shifted to 72.25 eV after the sample was exposed to  $1 \times 10^{-4}$  Torr CO (spectra ii) as CO molecules bind to the surface Pt atoms, while the subsurface Pt atoms are unaffected by the presence of CO. This pressure of CO is not high enough to induce any significant segregation of Pt atoms to the surface. $^{38}$ 

A thin Cu<sub>2</sub>O layer is typically prepared by annealing a Cu(111) surface at low pressures of  $O_2$  ( $10^{-7}$  to  $10^{-6}$  Torr) to produce either the "44" oxide at 473-623 K or the "29" oxide at 650 K. 46,47,49 For PtCu(111) single-atom alloys (SAAs), annealing at these temperatures in O2 causes the diffusion of Pt to the Cu bulk, 50 resulting in a complete loss of any detectable Pt in the surface or subsurface layers. Therefore, we used a lower temperature of 400 K to prepare a Cu<sub>2</sub>O layer over our PtCu(111) SAAs. Cu 2p XPS shown in Figure S1 shows a slightly increased intensity in the weak satellite feature at 942-948 eV indicating the formation of Cu<sup>+</sup> at 400 K, as was also observed for the "29" Cu<sub>2</sub>O layer prepared at 650 K. The O 1s peak of Cu<sub>2</sub>O prepared at 400 K is also identical with that of the "29" Cu<sub>2</sub>O (Figure S1). This shows that the lower oxidation temperature produced a surface that is chemically similar to, although likely not structurally identical with, the "29" Cu2O layer prepared at 650 K.

The Pt  $4f_{7/2}$  peak of the oxidized sample measured under UHV is shown as spectra iii in Figure 1 for two separate oxidation times: 3 min (Figure 1A) and 20 min (Figure 1B). The plot of the O 1s peak area as a function of time during

oxidation is shown in Figure S2, showing that the longer oxidation time resulted in a more complete oxide. In both cases, a shift of the binding energy of the subsurface Pt component is observed from 71.4 to 71.3 eV after oxidation. A similar shift was previously reported for the PtCu(111) SAA as a result of heating to 450 K under both UHV and ambient pressures of  $\rm H_2$  and CO. This was suggested to be caused by a decreased compressive strain as subsurface Pt atoms are dispersed from step edges to the Cu lattice in the terraces.<sup>3</sup> Clear differences in the Pt 4f spectra can be observed with different oxidation times. For the 3 min oxidation, hereafter referred to as Pt/Cu<sub>2</sub>O(3 min), ~40% of the free surface Pt atoms remain (Figure 1A, spectrum iii), and they are accessible to CO adsorption at room temperature (Figure 1A, spectrum iv). On the other hand, for the 20 min oxidation, hereafter referred to as Pt/Cu<sub>2</sub>O(20 min), a single symmetrical peak is observed at 71.3 eV (Figure 1B, spectrum iii), which is unchanged after the surface was exposed to  $1 \times 10^{-4}$  Torr of CO (Figure 1B, spectrum iv), indicating that the Pt atoms are inaccessible to CO adsorption. Because only one symmetrical 4f<sub>7/2</sub> peak is observed for Pt/Cu<sub>2</sub>O(20 min) and its binding energy is identical with that of subsurface Pt in metallic Pt/ Cu(111) SAA after heating, it is likely that the Pt atoms under the oxide layer have the same binding energy as subsurface Pt atoms in metallic PtCu(111). The total Pt 4f peak areas after oxidation are ~74% and ~67% of the initial Pt 4f peak area for the Pt/Cu<sub>2</sub>O(3 min) and Pt/Cu<sub>2</sub>O(20 min) surfaces, respectively. The lower overall amount of Pt detectable by XPS indicates that some of the Pt atoms diffuse more deeply into the metallic Cu bulk during the oxidation process.

The reduction of  $Cu_2O$  by  $H_2$  is known to be a very slow process at room temperature with a long induction time due to the high activation energy for  $H_2$  dissociation on the  $Cu_2O$  surface. In order to monitor the evolution of the oxide during its reduction under 1 Torr of  $H_2$ , we plotted in Figure 2A the O 1s peak areas for various  $Cu_2O$  surfaces as a function of time during the reduction by  $H_2$ . For the bare  $Cu_2O/Cu(111)$  surface, shown as solid circles, only a 10% decrease in the oxide peak intensity was observed after 2 h. The reduction

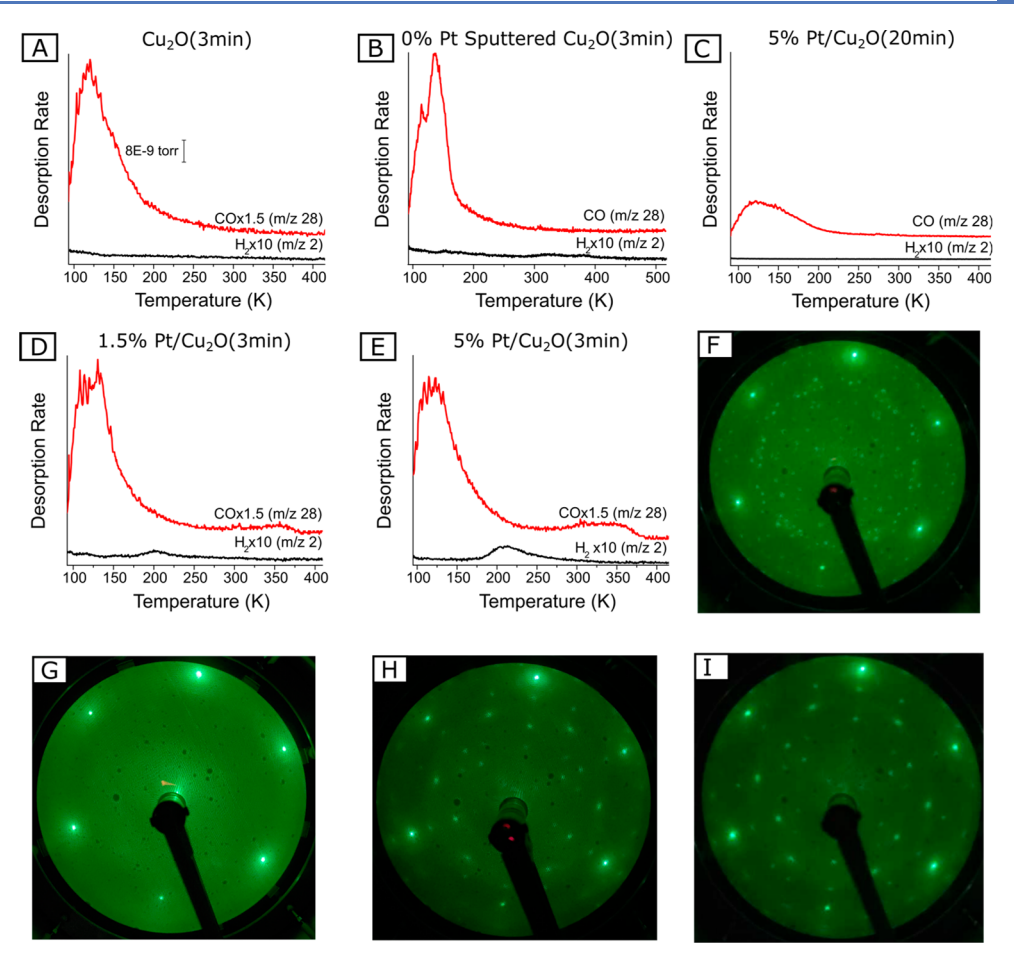


Figure 3. TPD profiles showing  $H_2$  desorption after a 100 L  $H_2$  exposure and CO desorption after a 20 L CO exposure of various "29"-like  $Cu_2O$  and  $Pt/Cu_2O$  surfaces with accompanying LEED patterns. The  $H_2$  and CO traces are from separate experiments but are plotted together. (A) Bare "29"-like  $Cu_2O(3 \text{ min})$ . (B) Bare "29" like  $Cu_2O(3 \text{ min})$  after being  $Ar^+$  sputtered for 60 s at 500 V. (C) 5%  $Pt/Cu_2O(20 \text{ min})$  surface. (D) 1.5%  $Pt/Cu_2O(3 \text{ min})$  surface. (E) 5%  $Pt/Cu_2O(3 \text{ min})$  surface. LEED patterns (F)–(I) correspond to experiments (A), (B), (D), and (E), respectively.

of Cu<sub>2</sub>O to metallic Cu by CO and CH<sub>3</sub>OH is known to start on step edges and defects. S1,52 Defect sites on the Cu<sub>2</sub>O surface have also been found by DFT calculations to decrease the activation energy for H<sub>2</sub> dissociation. To investigate the effect of defects on Cu<sub>2</sub>O reduction by H<sub>2</sub>, we prepared a defective Cu<sub>2</sub>O/Cu(111) surface by lightly sputtering a bare Cu<sub>2</sub>O layer with 5  $\times$  10 $^{-6}$  Torr of Ar at 500 V for 60 s, resulting in a 10% decrease in the oxide O 1s peak after sputtering. Figure 2A shows that the reduction of the defective Cu<sub>2</sub>O layer (open circles) occurs at a rate slightly faster than that of the pristine oxide (solid circles), likely due to the higher amounts of defects available for H<sub>2</sub> activation. However, 70% of the oxide remains after 2 h of H<sub>2</sub> exposure, indicating that the presence of defects only has a small effect on the reduction of the Cu<sub>2</sub>O layer.

The addition of Pt to Cu(111) prior to oxidation significantly accelerates the reduction of  $Cu_2O$ . For the 20 min oxide, a complete reduction of the oxide was observed in 80 min for 5% Pt and 2 h for 1.5% Pt. In both cases of the 20 min oxide, an induction period is observed at the beginning of the reduction, lasting  $\sim 50$  and 70 min for the 5% and 1.5% initial Pt coverages, respectively, during which the reduction proceeded very slowly. For the 3 min oxide, no induction time was observed, and reduction of the oxide was initiated immediately after the introduction of  $H_2$ , resulting in a

complete reduction in ~30 min. The O 1s spectra for the 5% Pt/Cu<sub>2</sub>O(3 min) sample measured in situ during reduction in H<sub>2</sub> are shown in Figure 2B, while the spectra for the reduction of the bare Cu<sub>2</sub>O, sputtered Cu<sub>2</sub>O, and the Pt/Cu<sub>2</sub>O(20 min) surfaces are shown in Figure S3. The remaining broad peak at ~531.5 eV after the oxide was completely reduced can be assigned to OH species, likely due to the dissociation of background water adsorbed on the surface, which is already present on the oxidized surface prior to reduction, as shown by the tail on the higher binding energy side of the oxide O 1s peak. We did not see evidence for the formation of water produced from the reaction between H and the lattice oxide O atoms, which likely immediately desorbed from the surface. The faster reduction of the Cu<sub>2</sub>O surface with the presence of Pt is conclusive evidence that Pt plays an important role in facilitating the reduction of Cu<sub>2</sub>O beyond the presence of any structural defects on the Cu2O surface introduced by the Pt atoms. For Pt/Cu<sub>2</sub>O(3 min), the faster reduction of Cu<sub>2</sub>O can be attributed to the presence of surface metallic Pt atoms, which are active for H<sub>2</sub> dissociation. However, the reduction mechanism is less straightforward for the Pt/Cu<sub>2</sub>O(20 min) surfaces, since the Pt atoms are likely covered by the Cu<sub>2</sub>O layer and thus are not accessible to H2 adsorption and dissociation.

The Pt  $4f_{7/2}$  spectra of the surface after the oxide was completely reduced are shown as spectra v in Figure 1A,B. The spectra were measured under  $1\times 10^{-4}$  Torr of CO at 300 K to probe the presence of surface Pt atoms. The CO-bound surface Pt component is observed after reduction of both the 3 and 20 min oxides with an intensities of 30% and 26% of the initial preoxidation value, respectively. The Cu 2p satellite feature, shown in Figure S1, decreased in intensity after the oxide was reduced, confirming the metallic state of Cu.

Modeling the  $Pt/Cu_2O$  SAA System with UHV Surface Science Methods. We utilized UHV surface science methods to further elucidate the active sites of the  $Pt/Cu_2O$  surface in order to understand the mechanism of enhanced  $Cu_2O$  reduction observed in the AP-XPS study, specifically the role of Pt in activating  $H_2$ . In order to model the AP-XPS experiments, corresponding PtCu(111) SAAs were prepared and subsequently oxidized at 400 K in  $O_2$  to form the same oxide thin film over the PtCu(111) alloy. To further understand the structure of these oxidized PtCu(111) alloys, we used a combination of LEED and CO TPD experiments before examining their ability to activate  $H_2$ .

Figure 3 presents a series of TPD and LEED data for various oxidized PtCu(111) surfaces. Figure 3A shows the results for a bare Cu sample after 3 min of oxidation. The LEED pattern displays long-range order akin to that of the "29" oxide. 53-55 Exposure of the surface to saturation CO at 85 K results in a CO desorption from the Cu<sub>2</sub>O layer at a temperature similar to that of the CO desorption from the "29" oxide. 56 This demonstrates that the oxide layer discussed throughout this paper is very similar to that in the previously studied "29" oxide. Figure 3A shows that saturation exposure of H<sub>2</sub> on the bare 3-min oxide did not result in any recombinative desorption of H<sub>2</sub>, indicating that the Cu<sub>2</sub>O surface is inactive for H<sub>2</sub> dissociation under these conditions. The surface studied in Figure 3B was prepared in the same manner as that studied in Figure 3A, but we introduced defect sites by sputtering the surface via Ar<sup>+</sup> ion bombardment. The LEED results show that the long-range order of the oxide has been disrupted and we only see the hexagonal array of spots indicative of Cu(111). Desorption of saturation CO from this surface displays features similar to CO desorption from Cu(111).<sup>25</sup> The amount of CO desorption is consistent before and after sputtering the "29"like oxide due to the difference in packing density of CO on Cu(111) vs. the "29" oxide. 56,57 Exposure of this sputtered surface to saturation H2 again results in negligible H2 desorption. This indicates that the defect sites are not highly active for H2 dissociation and do not have significant effects on the reduction of the oxide, consistent with the AP-XPS data presented in Figure 2A.

We now examine the effect of having small amounts of Pt alloyed into the Cu surface prior to oxidation. In Figure 3C, we begin by studying an oxidized 5% Pt/Cu<sub>2</sub>O(20 min) sample. The accompanying CO TPD trace only shows the low-temperature CO desorption features from the oxide layer and no high-temperature CO desorption from Pt sites. This is direct evidence that, after a 20 min oxidation period, the PtCu SAA sites are completely covered by the oxide. The H<sub>2</sub> TPD spectrum demonstrates that, when the surface is covered by an oxide layer, no H<sub>2</sub> dissociation occurs either. These findings are consistent with the AP-XPS experiments that show the presence of an induction period, during which the reduction of the oxide layer proceeds very slowly due to the lack of H<sub>2</sub> dissociation. In contrast, for the Pt/Cu<sub>2</sub>O(3 min) surface

(Figure 3D,E), we observe high-temperature CO desorption around 350 K after saturation CO exposure, which indicates the presence of exposed Pt sites for both the 1.5% and 5% initial Pt coverages. Because the packing densities of CO are different for the Cu(111) surface (0.52 ML of CO) and the "29" oxide surface (0.138 ML of CO), we cannot directly compare the total amount of CO desorbing from the substrate. 56,58 However, the packing density of CO on Pt is consistent across both of these samples. We are able to directly compare the CO desorption peaks at 350 K, which we attribute to CO desorption from Pt sites.<sup>36</sup> We find that there is more CO desorption from the Pt feature of the 5% Pt/Cu<sub>2</sub>O surface, indicating that there is more Pt accessible at higher initial coverages. The CO desorption peak from the Pt feature of the 1.5% Pt oxidized surface is 20% of the area of the CO desorption peak from Pt on the initial metallic PtCu(111) SAAs, indicating that the majority of the Pt atoms are still inaccessible to CO because they are located under the oxide layer, which is consistent with XPS data. This CO desorption behavior is similar to that of the PtCu(111) SAA, suggesting that the smaller fraction of exposed Pt sites still exist as single atoms that may sit at pores in the oxide layer or cause a restructuring of the oxide layer. 28 Examination of the LEED patterns also shows that the presence of Pt has caused the oxide to reconstruct. When the LEED pattern in Figure 3F is compared to those of Figure 3H,I, there are no overlapping diffraction spots. This supports the theory that the presence of Pt in the substrate can cause short-range restructuring of the oxide. For the LEED patterns with Pt present, the spots are farther apart from each other, signifying that the short-range order of this surface is not the same as that of the bare oxide layer.

In contrast to the bare Cu<sub>2</sub>O and Pt/Cu<sub>2</sub>O(20 min) surfaces, the Pt/Cu<sub>2</sub>O(3 min) surfaces are capable of dissociating H2 under the same experimental conditions. For both the 1.5% and 5% initial Pt coverages, recombinative desorption of H2 is observed around 200 K, similar to that from the metallic PtCu(111) SAA.<sup>28</sup> Again, the higher Pt coverages lead to more H2 dissociation. We can attribute this H<sub>2</sub> dissociation solely to the Pt sites in the surface, as revealed by the results shown in Figure S4, which demonstrate that, when 1.5% and 5% Pt/Cu<sub>2</sub>O(3 min) surfaces are prepared and saturated with CO at 200 K to poison any Pt sites, the surface becomes inactive for H<sub>2</sub> dissociation. This confirms that the active sites for H2 dissociation are the same Pt atoms that bind CO. Together, these results indicate that adding small amounts of Pt to the Cu(111) surface before the oxide is formed provides active Pt sites for H2 dissociation, a key step in the reduction of Cu<sub>2</sub>O.

**DFT-Based Model Studies.**  $H_2$  Activation. The oxidized PtCu(111) surface was found to be reducible in ambient-pressure experiments, and UHV studies indicated that these oxidized PtCu(111) surfaces must be able to dissociate  $H_2$ . Therefore, we sought to investigate this reaction through computational chemistry techniques on a model surface, informed by the previously described experiments so as to provide atomistic insights into these experimental results. The exact surface structure of the experimental system is unknown but has been shown to be structurally and electronically similar to that of the "29" oxide. A model for this surface, developed previously, was used as a starting point. The "29" oxide unit cell was modified for this study by swapping a Cu(111) substrate atom in one of the open oxide rings with a Pt atom,

effectively creating a PtCu(111) SAA under the oxide overlayer. This was done to simulate the oxidation of a PtCu(111) surface as opposed to a pure Cu(111) surface. Images of the original "29" oxide unit cell and modification are shown in Figure S5.

Our theoretical investigation began by computing the  $\rm H_2$  dissociation barriers over the Pt site in our Pt-alloyed "29" oxide model. Barriers for  $\rm H_2$  dissociation using our alloyed-Pt model are presented in Figure 4. Note that additional reaction

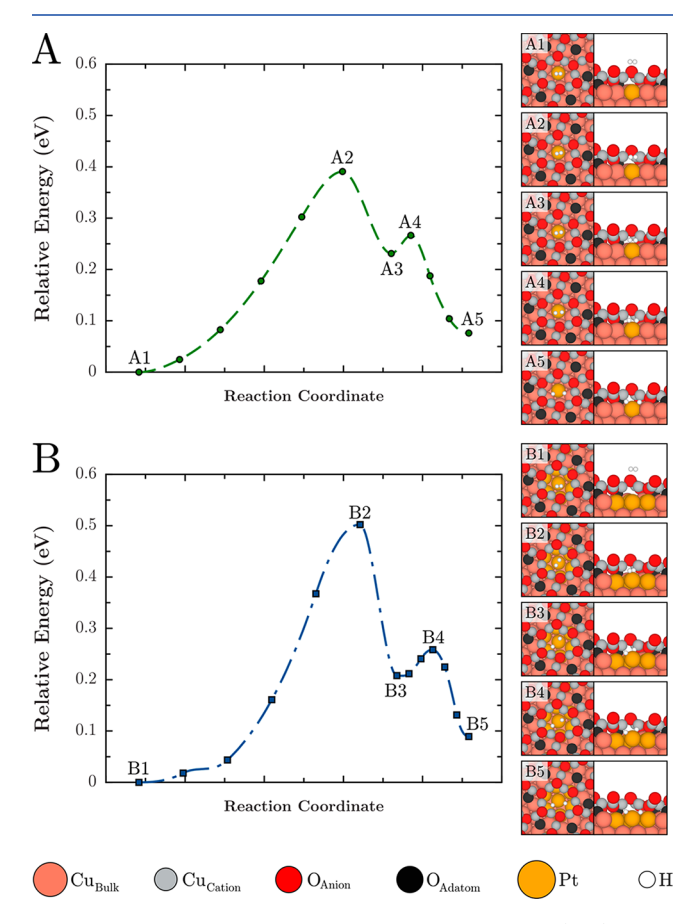


Figure 4.  $H_2$  theoretical reaction pathways over a PtCu(111) single atom (A) and seven-atom Pt alloy patch (B) beneath a "29" copper oxide overlayer. For comparison, the  $H_2$  dissociation barrier over a clean PtCu(111) alloy is approximately 0.05 eV.<sup>28,59</sup>

pathways involving surface hydroxyl formation were considered, but their activation energies were higher than those of the pathways presented in Figure 4 (see Figure S7). Figure 4A demonstrates that the barrier for H2 dissociation over the Pt atom alloyed in our "29" oxide model is not insignificant with an overall barrier of approximately 0.4 eV. While this is certainly more energetically favorable than dissociation over pure Cu<sub>2</sub>O surfaces,<sup>34</sup> it is significantly larger than H<sub>2</sub> activation barriers over Pt atoms in PtCu(111) SAAs, which have been estimated to be around 0.05 eV. 28,59 Replacement of additional Cu(111) substrate atoms with Pt around our initial substitution (to form a patch of Pt) did not lower the activation barrier (shown in Figure 4B). Further, both dissociation reactions in Figure 4 are endothermic, indicating that H<sub>2</sub> would likely desorb upon dissociation. Although the overall process of oxide reduction via H2 within our model is exothermic (shown by vacancy formation energies in Figure S11), the barrier calculations and endothermic dissociation

energy in Figure 4 allude to the difficulty of performing this first step in surface reduction on a surface with alloyed Pt densely surrounded by an oxide layer. A detailed analysis of H adsorption on our Pt-alloyed "29" oxide model that rationalizes this endothermic adsorption energy can be found in the Supporting Information.

O and CO Adsorption. In the previous section, we concluded that  $H_2$  activation over Pt atoms surrounded by  $Cu_2O$  (examined using a Pt-alloyed "29" oxide model) would be unlikely due to relatively high barriers and endothermic reaction energies. Therefore, we turned toward examining the interactions between the initial PtCu(111) SAA and oxygen. Adsorption energies of oxygen (with respect to oxygen in the gas phase) on Cu(111) and a PtCu(111) SAA, along with projected d band densities of states, are presented in Figure 5.

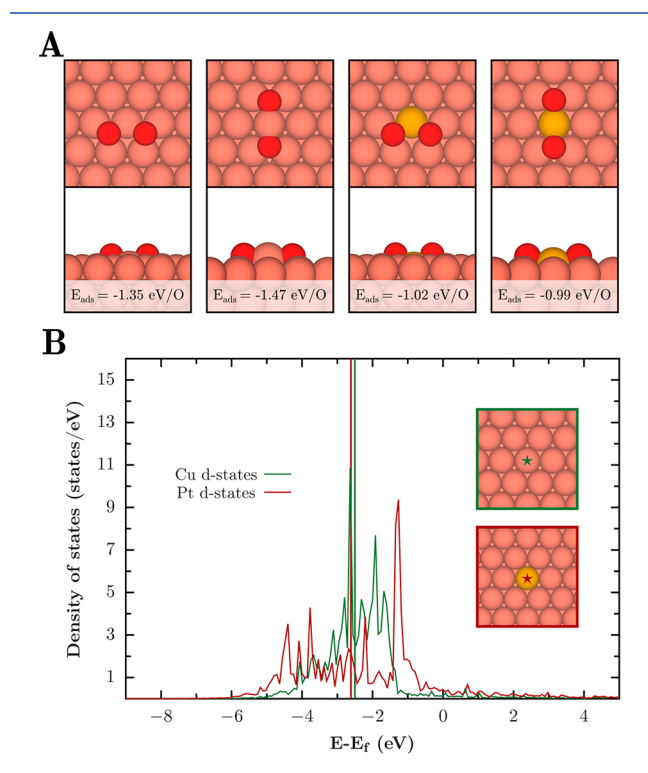


Figure 5. (A) Atomic structures of oxygen adsorption on Cu(111) and PtCu(111) along with (B) densities of states for the d bands of Cu and Pt (specific atom marked in figure) prior to oxygen adsorption. Band centers are marked with vertical lines and differ by approximately 0.11 eV (with Cu atoms being closer to the Fermi level).

The oxygen adsorption energies  $E_{\rm ads,O}$  presented in Figure 5 were calculated using the equation

$$E_{\text{ads,O}} = \frac{1}{2} (E_{\text{surface+2O}} - E_{\text{O}_{2,\text{gas}}} - E_{\text{surface}})$$
 (2)

In this equation,  $E_{\rm surface+2O}$  is the energy of the surface with two adsorbed oxygen atoms,  $E_{\rm surface}$  is the energy of the clean surface, and  $E_{\rm O_{1,ges}}$  is the energy of gas-phase oxygen. From Figure 5A, it is clear that oxygen binds significantly more weakly when it is coordinated to a Pt atom (along with coordination to neighboring Cu atoms) of the PtCu(111) SAA in comparison to pure Cu coordination when it is adsorbed on a Cu(111) surface. This can be rationalized through the d-band center adsorption model,  $^{60}$  as the d-band center for the

Pt atom of the SAA is slightly farther from the Fermi level than the surface Cu atoms of a Cu(111) surface (Figure 5B).

Figure S8 shows the adsorption energies of CO on a clean PtCu(111) SAA and our Pt-alloyed "29" oxide model. Adsorption of CO on the Pt site in our Pt-alloyed "29" oxide model (Figure S8B) is slightly weaker than adsorption on the bare "29" oxide in comparison with previous theoretical work.<sup>56</sup> Experimental work further demonstrates that CO desorbs from the bare "29" oxide below 200 K, 56 indicating that Pt sites densely surrounded by oxide could not be responsible for the CO desorption peaks at around 350 K seen in the TPD studies shown in Figure 3C,D. However, CO adsorbs much more strongly to a clean PtCu(111) SAA (Figure S8A), indicating that Pt sites surrounded by metallic Cu could be responsible for the high-temperature CO desorption peak observed experimentally.<sup>36</sup> This is likely due to the electronic repulsion between the CO molecule and the oxide layer, as can be seen on comparison of the contour lines of the electron density around CO on our Pt-alloyed "29" oxide model (Figure S8A) to that of the PtCu(111) SAA model (Figure S8B).

Effect of Alloyed Pt on Oxide Integrity. On the basis of experimental studies, a complete oxide layer is hypothesized to form over the PtCu(111) surface after the SAA was oxidized for 20 min. DFT-based calculations were performed to determine the effect of Pt alloyed into the underlying Cu(111) layer on the strength of Cu–O bonds in the oxide layer above. Oxygen vacancy formation energies,  $\Delta E_{\rm vac}$ , were calculated as the metric to quantify this bond strength within our "29" oxide model using the formula

$$\Delta E_{\text{vac}} = E_{\text{surf,vac}} + E_{\text{H}_2\text{O}} - E_{\text{surf,clean}} - E_{\text{H}_2}$$
(3)

In this equation,  $E_{\rm surf,vac}$  is the total energy of the surface with an O vacancy,  $E_{\rm surf,clean}$  is the total energy of the initial oxide surface, and  $E_{\rm H_2O}$  and  $E_{\rm H_2}$  are the total energies of gas-phase water and hydrogen, respectively. Note that as  $\Delta E_{\rm vac}$  decreases (i.e., becomes more negative), water formation using oxygen from the oxide becomes more thermodynamically favorable. This suggests that the bonds of the removed oxygen to the surrounding oxide also become weaker due to this increase in favorability.

The effect of alloyed Pt on the oxide bond strength was examined by first selecting an oxygen atom within our "29" oxide model in order to compute the vacancy formation energies. The vacancy formation energy for this oxygen was computed with Pt substituted for different Cu atoms in the top layer of the underlying Cu(111) substrate of our Pt-alloyed "29" oxide model. As there are 29 atoms per layer of the Cu(111) substrate, there were 29 vacancy formation energies computed. To compute these vacancy formation energies, a surface Cu(111) atom in the "perfect" "29" oxide unit cell was swapped for a Pt to compute  $E_{\text{surf,clean}}$  in the vacancy formation energy equation above. Next, the oxygen of interest was removed from this cell to compute  $E_{\text{surf,vac}}$  in the vacancy formation energy equation above. Our choice to not relax the structures here was intentional (i.e.,  $E_{\text{surf,vac}}$  and  $E_{\text{surf,clean}}$  are single-point calculations). This choice was made to deconvolute the effect of Pt on the oxide bond strength from any surface reconstruction that would occur following the formation of an oxygen vacancy. Not allowing the surface with a vacancy to relax allows  $\Delta E_{\rm vac}$  from eq 3 to solely measure the energetic cost of removing an oxygen from the

surface, and hence the oxide bond strength, without convolution from other phenomena. For calculations where the surface was allowed to relax to compute both  $E_{\rm surf,vac}$  and  $E_{\rm surf,vac}$  please see Figure S11.

Results for a single oxygen within our "29" oxide model are presented in Figure 6, where the oxygen for which vacancy

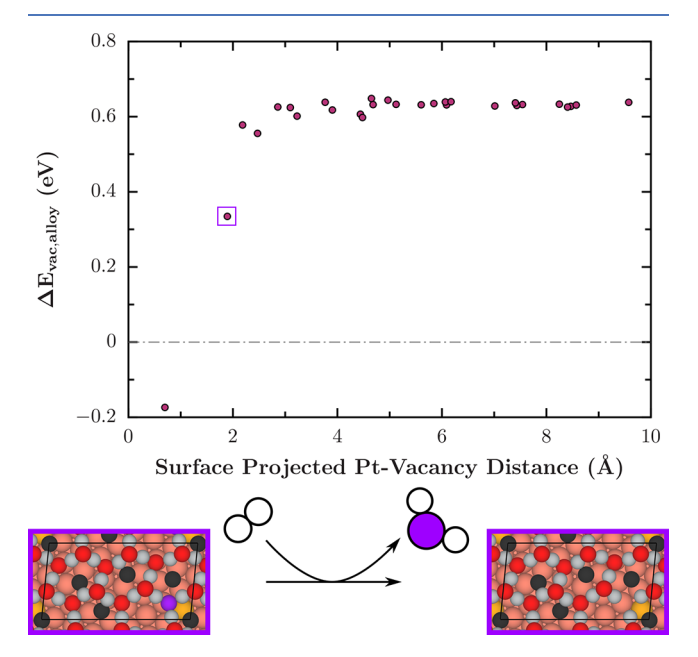


**Figure 6.** Oxygen vacancy formation energies from the "29" oxide model as a function of the surface-projected distance between the vacancy site and the Pt atom alloyed into the top Cu(111) layer of the atomistic model. Atomistic models are shown for this reaction using the alloy configuration of the data point marked with a purple square.

formation energies were computed is colored purple within the presented atomistic models. The results for additional oxygen are presented in the Supporting Information. From this figure, it is clear that, as the alloyed Pt is placed closer to the vacant oxygen site, the oxygen vacancy formation energy decreases. This suggests that alloyed Pt has a weakening effect on nearby Cu–O bonds, thus making direct reduction of the oxide via H<sub>2</sub> more feasible for oxygen anions that are near the alloyed Pt. A similar analysis was carried out for the formation of other oxygen vacancies in this Pt-alloyed "29" oxide model and is presented in Figure S9.

## DISCUSSION

Our experimental results clearly support the idea that the Pt dopant weakens the Cu–O bonds, as suggested by our DFT-based calculations that were discussed in the last section, as a short (3 min) oxidation time results in an incomplete oxide layer. CO adsorption on the  $Pt/Cu_2O(3 min)$  surface is observed by both XPS and TPD, which shows that patches of metallic Cu remain around the single Pt atoms, thereby allowing CO to adsorb on Pt. This provides a thermodynamic rationale for the presence of unoxidized Cu patches around the alloyed Pt atoms. The presence of these metallic Cu patches around Pt also allows the facile dissociation of  $H_2$  on Pt and the subsequent spillover of atomic  $H_2$ , which promotes the immediate reduction of the surface oxide without an induction period, as observed in Figure 2A.

A longer oxidation time at 400 K is likely able to overcome the weak adsorption of O, resulting in the formation of a more complete oxide layer with no metallic Cu patches around the Pt atoms, as evidenced by the absence of CO adsorption on the Pt/Cu<sub>2</sub>O(20 min) surface at room temperature. This is fully consistent with the DFT results, which show the weak adsorption energy of CO on the oxide-covered Pt sites. Consequently, H<sub>2</sub> cannot be activated on the Pt/Cu<sub>2</sub>O(20 min) surface, as shown by the absence of recombinative desorption of H2 in TPD as well as the high H2 dissociation barrier from the DFT calculations. The presence of chemisorbed O atoms on Pt sites can be ruled out, since any chemisorbed O would have immediately reacted with CO under our XPS and TPD experimental conditions shown in Figures 1 and 3,61,62 which would have then resulted in the adsorption of CO on Pt, which was not observed. The existence of an induction period in the initial stages of the reduction of the Pt/Cu<sub>2</sub>O(20 min) surface is a direct effect of this high barrier for H<sub>2</sub> dissociation. However, the Pt atoms under the oxide layer likely play an indirect role in initiating the oxide reduction. During the induction period, oxide reduction likely starts in the vicinity of the Pt atoms, since DFT calculations show that the presence of Pt in the underlying metallic layer under the oxide weakens neighboring Cu-O bonds. The initial reduction is a slow process due to the high barrier for H<sub>2</sub> dissociation, but even on a pristine Cu<sub>2</sub>O surface, oxide reduction has been found to start on defect sites. The Pt atoms in this case create defects in the oxide, which consequently help initiate the reduction. When enough metallic Cu atoms are formed around a Pt atom, the surface starts to resemble that of the 3 min oxide, and the reaction is significantly accelerated as the Pt atoms are able to play a direct role in H2 activation and spillover.

In Figure 2A, the slope of the O 1s peak area during reduction of the 5% Pt/Cu<sub>2</sub>O(3 min) surface is 0.039 min which is very similar to the slope of 0.037 min<sup>-1</sup> for the 5% Pt/ Cu<sub>2</sub>O(20 min) surface after the initial ~50 min of the induction period. This is evidence that the surface chemistry and reactivity of the 20 min oxide after the induction period is over are similar to those of the 3 min oxide with the same initial coverage of Pt. The postreduction surface of the 20 min oxide is also similar to that of the 3 min oxide with the same initial Pt coverage (Figure 1, spectra v), further giving evidence that, although initially all of the Pt atoms are covered by an oxide layer, a fraction of them (~25% of the initial amount) are exposed and available for CO adsorption after the oxide is reduced. The fact that the slope for the reduction of the 1.5% Pt/Cu<sub>2</sub>O surface after the induction period (i.e., after ~70 min) is less than half (0.017 min<sup>-1</sup>) of those for both 5% Pt/ Cu<sub>2</sub>O surfaces shows the direct role of Pt in facilitating the oxide reduction during this second stage of the reduction, as more Pt atoms result in a faster reaction. This is in agreement with the TPD data, which show a higher dissociation and uptake of H<sub>2</sub> for a higher amount of Pt. The shorter induction period for the 5% Pt/Cu<sub>2</sub>O(20 min) surface in comparison to the 1.5% Pt/Cu<sub>2</sub>O(20 min) surface indicates that Pt has an indirect role in the initial stages of the reduction, as there is a higher number of weaker Cu-O bonds induced by the presence of Pt.

### CONCLUSION

This work presents a powerful combination of *in situ* ambient-pressure and UHV experiments with DFT-based calculations that sheds light on  $\rm H_2$  dissociation and oxide reduction at metal/oxide interfaces promoted by the presence of small

amounts of isolated noble metals. Both XPS and TPD data show that a fully oxidized PtCu(111) SAA surface has no accessible surface Pt sites, as evidenced by the absence of CO adsorption on Pt at room temperature. This surface is also inactive for H2 activation, as confirmed by our DFT-based analysis and the slow initial reduction of the overlying oxide layer. However, a computational model indicates that the presence of Pt weakens Cu-O bonds in its vicinity, which means that the Pt/Cu<sub>2</sub>O interface plays an important role in initiating the reduction of oxide around it despite the fact that the Pt atoms initially do not directly dissociate H2. A partial reduction of the full oxide layer results in a surface with exposed surface Pt atoms surrounded by patches of metallic Cu. This surface can also be prepared by oxidizing the PtCu(111) SAA surface for a shorter time. These exposed surface Pt sites are highly active in dissociating H2, which consequently accelerate the reduction of the oxide layer.

Therefore, the reduction of a fully oxidized PtCu(111) SAA surface occurs in two phases. First, since no surface Pt atoms are initially available for  $H_2$  dissociation, the initial stage of reduction during the induction period proceeds slowly. The reduction starts with weaker Cu–O bonds directly in the vicinity of the Pt atom, creating patches of metallic Cu around Pt. The exposed Pt atom then becomes highly active for  $H_2$  dissociation and plays a direct role in catalyzing the second phase of the reduction, during which the reduction becomes much faster. It should be noted that, for an initial 1.5% surface Pt coverage, the amount of exposed surface Pt atoms in the second phase of the reduction is much lower ( $\sim$ 25% of the initial amount, corresponding to  $\sim$ 0.4% surface coverage). Yet this minute amount of Pt is enough to significantly accelerate the reduction of the Cu<sub>2</sub>O layer.

This finding has important implications in catalysis, since the seemingly inert oxide-covered PtCu SAA is actually able to promote the reduction of the oxide due to the presence of dopant single Pt atoms under the oxide, thus creating nucleation sites for the formation of metallic Cu. These insights into the reactivity of metal/oxide interface sites toward  $\rm H_2$  activation and their effect on the subsequent reduction of the oxide can be used in rational catalyst design efforts for reactions where interface regions are key to high activity and prone to deactivation. For Cu-based methanol synthesis catalysts, for example, the addition of a small amount of Pt dopant, at the single-atom limit, could provide a way to maintain a reduced state of Cu under relatively mild reaction conditions where  $\rm H_2$  dissociation may be rate limiting.

## ASSOCIATED CONTENT

## **Solution** Supporting Information

The Supporting Information is available free of charge at https://pubs.acs.org/doi/10.1021/acscatal.9b05270.

Further discussion on H adsorption and  $H_2$  dissociation on the  $Pt/Cu_2O$  model system,  $Cu\ 2p\ XPS$  spectra before and after oxidation and after reduction,  $O\ 1s\ XPS$  spectra and plot of oxide peak area during oxidation of Pt/Cu(111),  $O\ 1s\ XPS$  spectra waterfall plots during  $Cu_2O$  reduction, TPD data with coadsorbed  $H_2$  and CO, atomic structure of the "29" oxide model, and additional DFT results on d-band analysis of H adsorption on Pt, the reaction pathway for  $H_2$  dissociation, CO adsorption energy on Pt,  $O\ vacancy$  formation energy, and

computed Bader charges along  $H_2$  dissociation pathways (PDF)

Crystallographic data for the DFT-based structures (CIF)

## AUTHOR INFORMATION

#### **Corresponding Authors**

Jean-Sabin McEwen — The Gene and Linda Voiland School of Chemical Engineering and Bioengineering, Department of Physics and Astronomy, Department of Chemistry, and Department of Biological Systems Engineering, Washington State University, Pullman, Washington 99164, United States; Institute for Integrated Catalysis, Pacific Northwest National Laboratory, Richland, Washington 99352, United States; orcid.org/0000-0003-0931-4869; Email: js.mcewen@wsu.edu

E. Charles H. Sykes — Department of Chemistry, Tufts University, Medford, Massachusetts 02155, United States; Email: charles.sykes@tufts.edu

Iradwikanari Waluyo — National Synchrotron Light Source II, Brookhaven National Laboratory, Upton, New York 11973, United States; orcid.org/0000-0002-4046-9722; Email: iwaluyo@bnl.gov

## Authors

Alex C. Schilling – Department of Chemistry, Tufts University, Medford, Massachusetts 02155, United States

**Kyle Groden** – The Gene and Linda Voiland School of Chemical Engineering and Bioengineering, Washington State University, Pullman, Washington 99164, United States

Juan Pablo Simonovis — National Synchrotron Light Source II, Brookhaven National Laboratory, Upton, New York 11973, United States

Adrian Hunt — National Synchrotron Light Source II, Brookhaven National Laboratory, Upton, New York 11973, United States

Ryan T. Hannagan — Department of Chemistry, Tufts University, Medford, Massachusetts 02155, United States Volkan Çınar — Department of Chemistry, Tufts University, Medford, Massachusetts 02155, United States

Complete contact information is available at: https://pubs.acs.org/10.1021/acscatal.9b05270

## **Author Contributions**

OA.C.S. and K.G. contributed equally.

#### Notes

The authors declare no competing financial interest.

## ACKNOWLEDGMENTS

This research used resources of the 23-ID-2 (IOS) beamline of the National Synchrotron Light Source II, a U.S. Department of Energy (DOE) Office of Science User Facility operated for the DOE Office of Science by Brookhaven National Laboratory under Contract No. DE-SC0012704. J.P.S. is supported through the NSLS-II Director's Postdoctoral Program jointly with the BNL Chemistry Division. All UHV

work was perfomed at Tufts and was supported by the Catalysis Science Program at the Department of Energy BES under Grant No. DE-FG02-05ER15730. Financial support to WSU was provided by the National Science Foundation CAREER program under Contract No. CBET-1653561. All computational work was performed using resources at EMSL, a national scientific user facility sponsored by the Department of Energy's Office of Biological and Environmental Research and located at PNNL. PNNL is a multiprogram national laboratory operated for the U.S. DOE by Battelle.

## DEDICATION

We wish to dedicate this paper to the memory of our dear friend and colleague Maria Flytzani-Stephanopoulos.

## **■** REFERENCES

- (1) Guil-López, R.; Mota, N.; Llorente, J.; Millán, E.; Pawelec, B.; García, R.; Fierro, J. L. G.; Navarro, R. M. Structure and Activity of Cu/ZnO Catalysts Co-Modified with Aluminium and Gallium for Methanol Synthesis. *Catal. Today* **2019**, *24*, 104010.
- (2) Economic and Employment Impacts of U.S. Methanol Industry; ADI Analytics: Houston, TX, 2017.
- (3) US Methanol LLC. Welcome to US Methanol; https://www.usmeoh.com/ (accessed June 4, 2019).
- (4) Jung, K. D.; Bell, A. T. Role of Hydrogen Spillover in Methanol Synthesis over Cu/ZrO<sub>2</sub>. *J. Catal.* **2000**, *193*, 207–223.
- (5) Witoon, T.; Kachaban, N.; Donphai, W.; Kidkhunthod, P.; Faungnawakij, K.; Chareonpanich, M.; Limtrakul, J. Tuning of Catalytic CO<sub>2</sub> Hydrogenation by Changing Composition of CuOZnO-ZrO<sub>2</sub> Catalysts. *Energy Convers. Manage.* **2016**, *118*, 21–31.
- (6) Phongamwong, T.; Chantaprasertporn, U.; Witoon, T.; Numpilai, T.; Poo-Arporn, Y.; Limphirat, W.; Donphai, W.; Dittanet, P.; Chareonpanich, M.; Limtrakul, J. CO<sub>2</sub> Hydrogenation to Methanol over CuO-ZnO-ZrO<sub>2</sub>-SiO<sub>2</sub> Catalysts: Effects of SiO<sub>2</sub> Contents. *Chem. Eng. J.* **2017**, *316*, 692–703.
- (7) Arena, F.; Italiano, G.; Barbera, K.; Bordiga, S.; Bonura, G.; Spadaro, L.; Frusteri, F. Solid-State Interactions, Adsorption Sites and Functionality of Cu-ZnO/ZrO<sub>2</sub> Catalysts in the CO<sub>2</sub> Hydrogenation to CH<sub>3</sub>OH. *Appl. Catal., A* **2008**, *350*, 16–23.
- (8) van den Berg, R.; Prieto, G.; Korpershoek, G.; van der Wal, L. I.; van Bunningen, A. J.; Lægsgaard-Jørgensen, S.; de Jongh, P. E.; de Jong, K. P. Structure Sensitivity of Cu and CuZn Catalysts Relevant to Industrial Methanol Synthesis. *Nat. Commun.* **2016**, *7*, 13057.
- (9) Wang, Y.; Kattel, S.; Gao, W.; Li, K.; Liu, P.; Chen, J. G.; Wang, H. Exploring the Ternary Interactions in Cu-ZnO-ZrO<sub>2</sub> Catalysts for Efficient CO<sub>2</sub> Hydrogenation to Methanol. *Nat. Commun.* **2019**, *10*, 1166.
- (10) Thorhauge, M.; Kuld, S.; Chorkendorff, I.; Falsig, H.; Elkjaer, C. F.; Helveg, S.; Sehested, J. Quantifying the Promotion of Cu Catalysts by ZnO for Methanol Synthesis. *Science* **2016**, 352, 969–974.
- (11) Günter, M. M.; Ressler, T.; Bems, B.; Büscher, C.; Genger, T.; Hinrichsen, O.; Muhler, M.; Schlögl, R. Implication of the Microstructure of Binary Cu/ZnO Catalysts for Their Catalytic Activity in Methanol Synthesis. *Catal. Lett.* **2001**, *71*, 37–44.
- (12) Rasmussen, P. B.; Holmblad, P. M.; Askgaard, T.; Ovesen, C. V.; Stoltze, P.; Norskov, J. K.; Chorkendorff, I. Methanol Synthesis on Cu(100) from a Binary Gas Mixture of CO<sub>2</sub> and H<sub>2</sub>. *Catal. Lett.* **1994**, 26, 373–381.
- (13) Burch, R.; Golunski, S. E.; Spencer, M. S. The Role of Copper and Zinc Oxide in Methanol Synthesis Catalysts. *J. Chem. Soc., Faraday Trans.* **1990**, *86*, 2683–2691.
- (14) Spencer, M. S. Role of ZnO in Methanol Synthesis on Copper Catalysts. *Catal. Lett.* **1998**, *50*, 37–40.
- (15) Wagner, J. B.; Hansen, P. L.; Molenbroek, A. M.; Topsøe, H.; Clausen, B. S.; Helveg, S. *In Situ* Electron Energy Loss Spectroscopy

- Studies of Gas-Dependent Metal-Support Interactions in Cu/ZnO Catalysts. J. Phys. Chem. B 2003, 107, 7753-7758.
- (16) Jedrecy, N.; Gallini, S.; Sauvage-Simkin, M.; Pinchaux, R. Copper Growth on the O-Terminated ZnO (0001)Surface: Structure and Morphology. *Phys. Rev. B: Condens. Matter Mater. Phys.* **2001**, *64*, 085424.
- (17) Kniep, B.; Kasatkin, I.; Kurr, P.; Schlögl, R.; Trunschke, A. Role of Lattice Strain and Defects in Copper Particles on the Activity of Cu/ZnO/Al<sub>2</sub>O<sub>3</sub> Catalysts for Methanol Synthesis. *Angew. Chem., Int. Ed.* **2007**, *46*, 7324–7327.
- (18) Bonura, G.; Cordaro, M.; Cannilla, C.; Arena, F.; Frusteri, F. The Changing Nature of the Active Site of Cu-Zn-Zr Catalysts for the CO<sub>2</sub> Hydrogenation Reaction to Methanol. *Appl. Catal., B* **2014**, *152–153*, 152–161.
- (19) Kattel, S.; Liu, P.; Chen, J. G. Tuning Selectivity of CO<sub>2</sub> Hydrogenation Reactions at the Metal/Oxide Interface. *J. Am. Chem. Soc.* **2017**, 139, 9739–9754.
- (20) Kattel, S.; Ramírez, P. J.; Chen, J. G.; Rodriguez, J. A.; Liu, P. Active Sites for CO<sub>2</sub> Hydrogenation to Methanol on Cu/ZnO Catalysts. *Science* **2017**, 355, 1296–1299.
- (21) Tovar, M.; Kurr, P.; Schlögl, R.; Studt, F.; Kuhl, S.; Nørskov, J. K.; Fischer, R. W.; Behrens, M.; Kniep, B. L.; Zander, S.; Abild-Pedersen, F.; Kasatkin, I.; Girgsdies, F.; Havecker, M. The Active Site of Methanol Synthesis over Cu/ZnO/Al<sub>2</sub>O<sub>3</sub> Industrial Catalysts. *Science* **2012**, *336*, 893–897.
- (22) Poulain, C.; Wiame, F.; Maurice, V.; Marcus, P. Novel Nanostructuring of the O/Cu(110) Surface by Reaction to Oxygen. *Surf. Sci.* **2012**, *606*, L26–L30.
- (23) Gattinoni, C.; Michaelides, A. Atomistic Details of Oxide Surfaces and Surface Oxidation: The Example of Copper and Its Oxides. *Surface Science Reports*; North-Holland: 2015; pp 424–447.
- (24) Lian, X.; Xiao, P.; Yang, S. C.; Liu, R.; Henkelman, G. Calculations of Oxide Formation on Low-Index Cu Surfaces. *J. Chem. Phys.* **2016**, *145*, 044711.
- (25) Lucci, F. R.; Darby, M. T.; Mattera, M. F. G.; Ivimey, C. J.; Therrien, A. J.; Michaelides, A.; Stamatakis, M.; Sykes, E. C. H. Controlling Hydrogen Activation, Spillover, and Desorption with Pd-Au Single-Atom Alloys. *J. Phys. Chem. Lett.* **2016**, *7*, 480–485.
- (26) Lucci, F. R.; Liu, J.; Marcinkowski, M. D.; Yang, M.; Allard, L. F.; Flytzani-Stephanopoulos, M.; Sykes, E. C. H. Selective Hydrogenation of 1,3-Butadiene on Platinum-Copper Alloys at the Single-Atom Limit. *Nat. Commun.* **2015**, *6*, 8550.
- (27) Lewis, E. A.; Marcinkowski, M. D.; Murphy, C. J.; Liriano, M. L.; Sykes, E. C. H. Hydrogen Dissociation, Spillover, and Desorption from Cu-Supported Co Nanoparticles. *J. Phys. Chem. Lett.* **2014**, 5, 3380–3385.
- (28) Lucci, F. R.; Marcinkowski, M. D.; Lawton, T. J.; Sykes, E. C. H. H<sub>2</sub> Activation and Spillover on Catalytically Relevant Pt-Cu Single Atom Alloys. *J. Phys. Chem. C* **2015**, *119*, 24351–24357.
- (29) Kim, J. Y.; Rodriguez, J. A.; Hanson, J. C.; Frenkel, A. I.; Lee, P. L. Reduction of CuO and Cu<sub>2</sub>O with H<sub>2</sub>: H Embedding and Kinetic Effects in the Formation of Suboxides. *J. Am. Chem. Soc.* **2003**, *125*, 10684–10692.
- (30) Baber, A. E.; Xu, F.; Dvorak, F.; Mudiyanselage, K.; Soldemo, M.; Weissenrieder, J.; Senanayake, S. D.; Sadowski, J. T.; Rodriguez, J. A.; Matolín, V.; White, M. G.; Stacchiola, D. J. *In Situ* Imaging of Cu<sub>2</sub>O under Reducing Conditions: Formation of Metallic Fronts by Mass Transfer. *J. Am. Chem. Soc.* **2013**, *135*, 16781–16784.
- (31) Zhang, K.; Li, L.; Shaikhutdinov, S.; Freund, H. J. Carbon Monoxide Oxidation on Metal-Supported Monolayer Oxide Films: Establishing Which Interface Is Active. *Angew. Chem., Int. Ed.* **2018**, *57*, 1261–1265.
- (32) Eren, B.; Heine, C.; Bluhm, H.; Somorjai, G. A.; Salmeron, M. Catalyst Chemical State during CO Oxidation Reaction on Cu(111) Studied with Ambient-Pressure X-Ray Photoelectron Spectroscopy and Near Edge X-Ray Adsorption Fine Structure Spectroscopy. *J. Am. Chem. Soc.* **2015**, *137*, 11186–11190.
- (33) Waluyo, I.; Mudiyanselage, K.; Xu, F.; An, W.; Liu, P.; Boscoboinik, J. A.; Rodriguez, J. A.; Stacchiola, D. J. Potassium-

- Promoted Reduction of Cu<sub>2</sub>O/Cu(111) by CO. *J. Phys. Chem. C* **2019**, 123, 8057–8066.
- (34) Zhang, R.; Wang, B.; Ling, L.; Liu, H.; Huang, W. Adsorption and Dissociation of  $H_2$  on the  $Cu_2O(111)$  Surface: A Density Functional Theory Study. *Appl. Surf. Sci.* **2010**, 257, 1175–1180.
- (35) Kim, M.; Pan, L.; Weaver, J. F.; Asthagiri, A. Initial Reduction of the PdO(101) Surface: Role of Oxygen Vacancy Formation Kinetics. *J. Phys. Chem. C* **2018**, *122*, 26007–26017.
- (36) Darby, M. T.; Lucci, F. R.; Marcinkowski, M. D.; Therrien, A. J.; Michaelides, A.; Stamatakis, M.; Sykes, E. C. H. Carbon Monoxide Mediated Hydrogen Release from PtCu Single-Atom Alloys: The Punctured Molecular Cork Effect. *J. Phys. Chem. C* **2019**, *123*, 10419–10428.
- (37) Therrien, A. J.; Zhang, R.; Lucci, F. R.; Marcinkowski, M. D.; Hensley, A.; McEwen, J.-S.; Sykes, E. C. H. Structurally Accurate Model for the "29"-Structure of  $Cu_xO/Cu(111)$ : A DFT and STM Study. *J. Phys. Chem. C* **2016**, *120*, 10879–10886.
- (38) Simonovis, J. P.; Hunt, A.; Palomino, R. M.; Senanayake, S. D.; Waluyo, I. Enhanced Stability of Pt-Cu Single-Atom Alloy Catalysts: *In Situ* Characterization of the Pt/Cu(111) Surface in an Ambient Pressure of CO. *J. Phys. Chem. C* **2018**, *122*, 4488–4495.
- (39) Gellman, A. J. Chiral Surfaces: Accomplishments and Challenges. ACS Nano 2010, 4, 5-10.
- (40) Kresse, G.; Hafner, J. Ab Initio Molecular Dynamics for Liquid Metals. *Phys. Rev. B: Condens. Matter Mater. Phys.* **1993**, 47, 558–561.
- (41) Kresse, G.; Furthmüller, J. Efficient Iterative Schemes for *Ab Initio* Total-Energy Calculations Using a Plane-Wave Basis Set. *Phys. Rev. B: Condens. Matter Mater. Phys.* **1996**, *54*, 11169–11186.
- (42) Blöchl, P. E. Projector Augmented-Wave Method. *Phys. Rev. B: Condens. Matter Mater. Phys.* **1994**, *50*, 17953–17979.
- (43) Perdew, J. P.; Burke, K.; Ernzerhof, M. Generalized Gradient Approximation Made Simple. *Phys. Rev. Lett.* **1996**, 77, 3865–3868.
- (44) Henkelman, G.; Jónsson, H. Improved Tangent Estimate in the Nudged Elastic Band Method for Finding Minimum Energy Paths and Saddle Points. *J. Chem. Phys.* **2000**, *113*, 9978–9985.
- (45) Henkelman, G.; Uberuaga, B. P.; Jónsson, H. A Climbing Image Nudged Elastic Band Method for Finding Saddle Points and Minimum Energy Paths. *I. Chem. Phys.* **2000**, *113*, 9901–9904.
- (46) Matsumoto, T.; Bennett, R. A.; Stone, P.; Yamada, T.; Domen, K.; Bowker, M. Scanning Tunneling Microscopy Studies of Oxygen Adsorption on Cu(111). *Surf. Sci.* **2001**, *471*, 225–245.
- (47) Jensen, F.; Besenbacher, F.; Stensgaard, I. Two New Oxygen Induced Reconstructions on Cu(111). *Surf. Sci.* **1992**, 269–270, 400–404.
- (48) Simonovis, J. P.; Hunt, A.; Senanayake, S. D.; Waluyo, I. Subtle and Reversible Interactions of Ambient Pressure  $\rm H_2$  with Pt/Cu(111) Single-Atom Alloy Surfaces. *Surf. Sci.* **2019**, *679*, 207–213.
- (49) Jensen, F.; Besenbacher, F.; Lægsgaard, E.; Stensgaard, I. Oxidation of Cu(111): Two New Oxygen Induced Reconstructions. *Surf. Sci.* 1991, 259, L774–L780.
- (50) Therrien, A. J.; Hensley, A. J. R.; Marcinkowski, M. D.; Zhang, R.; Lucci, F. R.; Coughlin, B.; Schilling, A. C.; McEwen, J. S.; Sykes, E. C. H. An Atomic-Scale View of Single-Site Pt Catalysis for Low-Temperature CO Oxidation. *Nat. Catal.* **2018**, *1*, 192–198.
- (51) Pollmann, S.; Bayer, A.; Ammon, C.; Steinruck, H. P. Adsorption and Reaction of Methanol on Clean and Oxygen Precovered Cu(111). Z. Phys. Chem. 2004, 218, 957–971.
- (52) Lawton, T. J.; Kyriakou, G.; Baber, A. E.; Sykes, E. C. H. An Atomic Scale View of Methanol Reactivity at the  $Cu(111)/CuO_x$  Interface. *ChemCatChem* **2013**, *5*, 2684–2690.
- (53) Matsumoto, T.; Bennett, R. A.; Stone, P.; Yamada, T.; Domen, K.; Bowker, M. Scanning Tunneling Microscopy Studies of Oxygen Adsorption on Cu(111). *Surf. Sci.* **2001**, *471*, 225–245.
- (54) Moritani, K.; Okada, M.; Teraoka, Y.; Yoshigoe, A.; Kasai, T. Reconstruction of Cu(111) Induced by a Hyperthermal Oxygen Molecular Beam. *J. Phys. Chem. C* **2008**, *112*, 8662–8667.
- (55) Wiame, F.; Maurice, V.; Marcus, P. Initial Stages of Oxidation of Cu(111). Surf. Sci. 2007, 601, 1193–1204.

- (56) Hensley, A. J. R.; Therrien, A. J.; Zhang, R.; Marcinkowski, M. D.; Lucci, F. R.; Sykes, E. C. H.; McEwen, J. S. CO Adsorption on the "29" Cu<sub>x</sub>O/Cu(111) Surface: An Integrated DFT, STM, and TPD Study. *J. Phys. Chem. C* **2016**, *120*, 25387–25394.
- (57) Kirstein, W.; Krüger, B.; Thieme, F. CO Adsorption Studies on Pure and Ni-Covered Cu(111) Surfaces. *Surf. Sci.* **1986**, *176*, 505–529.
- (58) Raval, R.; Parker, S. F.; Pemble, M. E.; Hollins, P.; Pritchard, J.; Chesters, M. A. FT-Rairs, EELS and LEED Studies of the Adsorption of Carbon Monoxide on Cu(111). *Surf. Sci.* **1988**, *203*, 353–377.
- (59) Fu, Q.; Luo, Y. Catalytic Activity of Single Transition-Metal Atom Doped in Cu(111) Surface for Heterogeneous Hydrogenation. *J. Phys. Chem. C* **2013**, *117* (28), 14618–14624.
- (60) Hammer, B.; Nørskov, J. K. Theoretical Surface Science and Catalysis—Calculations and Concepts. *Adv. Catal.* **2000**, *45*, 71–129. (61) Bashlakov, D. L.; Juurlink, L. B. F.; Koper, M. T. M.; Yanson, A. I. Subsurface Oxygen on Pt(111) and Its Reactivity for CO Oxidation. *Catal. Lett.* **2012**, *142* (1), 1–6.
- (62) Kinne, M.; Fuhrmann, T.; Zhu, J. F.; Whelan, C. M.; Denecke, R.; Steinrück, H. P. Kinetics of the CO Oxidation Reaction on Pt(111) Studied by *in Situ* High-Resolution x-Ray Photoelectron Spectroscopy. *J. Chem. Phys.* **2004**, *120* (15), 7113–7122.